ISSN 1846-6168 (Print), ISSN 1848-5588 (Online)
https://doi.org/10.17559/TV-20241017002069
Original scientific paper

Multi Parameter FEM Optimisation of I.C. Engine V-Twin Valve Spring Compression Tool

Josip CUMIN*, Dejan MARIĆ, Daniel NOVOSELOVIĆ, Tomislav ŠOLIĆ

Abstract: This article deals with FEM optimization of valve spring compression tool. The new modified tool presented here is advanced in design and features (as opposed to the later one). The presented tool design is made with goal of higher tool rigidity, lower mass, lower material cost, easier manipulation in cramped space and easier positioning on the cylinder head. The three parameters varied on three levels - design of experiments was utilized for the observation of response in the form of equivalent stress and maximal allowable displacement of the tool base material. Statistical analysis shows influential factors for the proposed mathematical models. In the last part of the paper, the tool with optimal parameters, stresses and maximal displacement is shown.It was concluded that S355J2 material with thickness of 5 mm is optimal for the tool construction due to the relatively high yielding stress as opposed to calculated stresses in the spring compression tool itself, and it gives a reasonably small elastic displacement of the tool which is not critical for the maintenance job itself.

Keywords: FEM; internal combustion engine (I.C.E.); statistical analysis; tool construction; V-twin

1 INTRODUCTION

Modern engines, internal combustion (IC) engines often utilize high compression ratio *CR* in order to maximize working efficiency. Carburetted motorcycles present at the market, usually have compression ratio ranging from 7:1 to 10,5:1 [1]. Due to strict ecological restrictions in the latest years, the I.C. engines are often designed with higher compression ratio (up to 13,5:1), and lean air/fuel (*A*/*F*) ratio, which leads to higher engine heating [2]. In order to do so, modern internal combustion engines operate on high octane gasoline (unleaded) fuels, or on alternative mix of gasoline and ethanol-based fuels [3-5]. The fuel preparation is done by fuel injection which is mandatory for high volumetric compression ratio engines [6]. With (often) lean *A*/*F* ratio, and high compression ratio, the engine operates at higher temperatures and requires sophisticated liquid cooling system. In the automotive industry, there is a constant rising usage trend for polymer materials, or polymer-composite materials [7, 8], and utilizing smart technologies for reduction of friction in moving components [9-11]. In thermally loaded I. C. engines the combination of high heat exposure, and exposure to different chemicals in oil causes polymer materials do deteriorate [12, 13], and it is especially the case for intake and exhaust valve stem oil seals which are submerged in hot oil. In order to replace valve stem oil seals, often the top end needs to be disassembled which requires a lot of manual labour and results in high maintenance expenses. This problem can be diagnosed through increased oil consumption, hesitant engine cold starting and by fouled spark plugs, and it can be diagnosed even in Do-It-Yourself (DIY) scheduled maintenance periods [14], and reliability can be assessed also [15]. Fig. 1 shows general example of V-twin engine configuration. In order to manually remove valve stem seals on this engine, the top end need to be disassembled completely which leads to higher repair costs and possible problems in reassembly process. There is also second repair plan - possibility of pressurising the cylinder on site, and compressing valve springs with top mounted compression tool. This paper presents multi-parameter optimisation of the previously made valve compression tool in order to achieve minimal stresses, and minimal displacement of the outside nodes in the tool under load. Fig. 2 shows 2D scan of the mating surface of V-twin engine head for which valve compression tool is made.

Figure 1 Example of V-twin engine

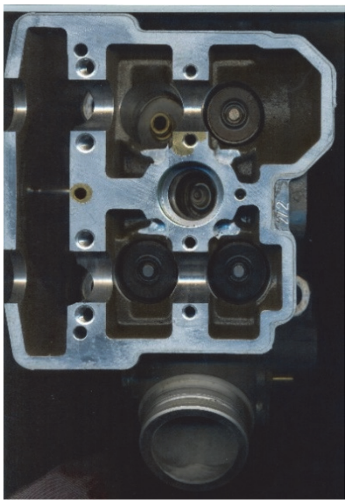

Figure 2 2D scan of the mating surface of V-twin engine head

2 DESIGN

Fig. 3 shows base plate design for the spring compression tool intended for V-twin cylinder head (from Fig. 2). Tab. 1. gives a general overview of the engine data specifications, with regard to thermal loads on the engine components and produced heat.

Table 1 I. C engine data overview / per cylinder

Working volume:	~ 471 ccm
Stroke/piston ratio:	100/60 (oversquare)
Power:	~ 50 HP
Compression ratio	11,5:1
Number of strokes:	4
Number of sparks:	1
Fuel type:	≥ RON 95
Valves per cylinder:	4

The tool was designed in such a way that it contacts only part of the cylinder head where threaded holes are accessible. The tool section covering the cam chain is not important structurally, it can only prevent falling of the small parts inside the engine, but technicians often use cotton rags exactly to prevent such occurrences.

It was also done for the purpose of retaining small tool mass, and for easier tool manipulation in tight spaces (Fig. 3).

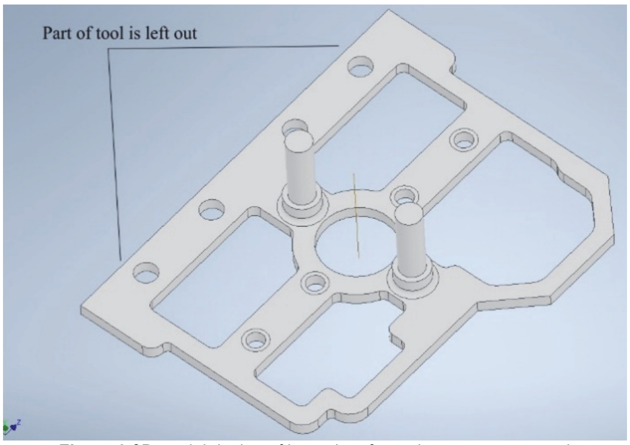

Figure 3 3D model design of baseplate for spring compressor tool

In order to proceed with multi parametric optimisation in Finite Element Method (FEM) environment of Autodesk Inventor, the spring force needs to be known. For this purpose, the used set of springs was subjected to compression testing in order to measure maximal spring force. Fig. 4 shows measuring equipment, and Fig. 5 shows obtained results.

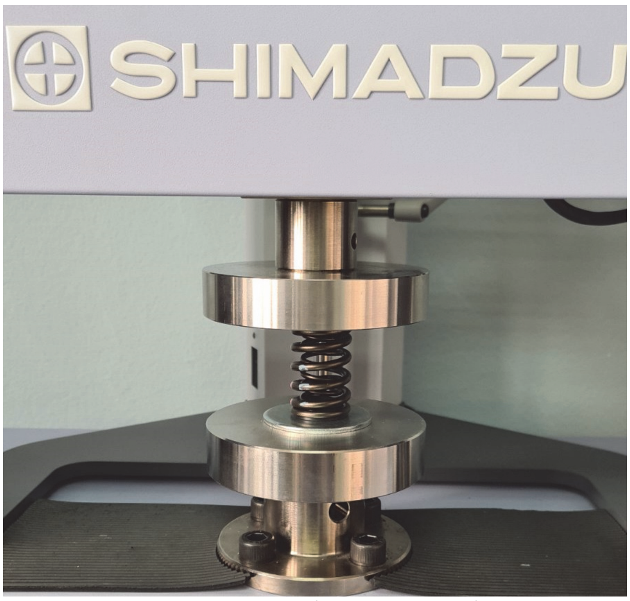

Figure 4 Measurement of valve compression force

The total measured force of fully compressed valve springs (outer and inner) was measured with Shimadzu AGS-10 X (Fig. 4) and it amounts to: F_s = 429 N for total spring displacement of u = 10,0 mm. Fig. 6 shows schematic of spring compression tool. It consists of the base plate shown in Fig. 3, welded screws, rigid cylinder with pivot point for rocker arm, and valve collar receiver which is connected to the rocker arm.

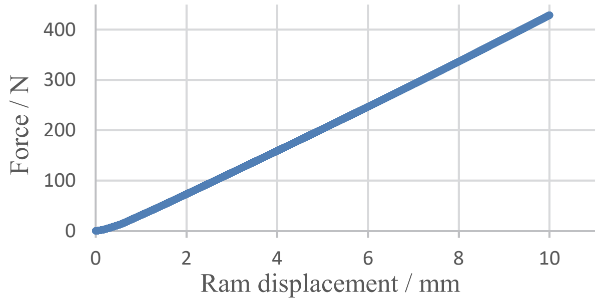

Figure 5 Total measured force for maximal spring compression

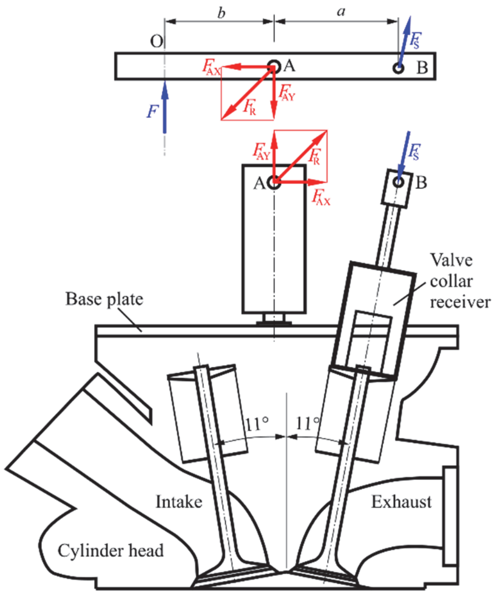

Figure 6 Spring compression tool schematic

If it is set that $\sum F_x = 0$, then it can be written:

$$-F_{AX} + F_S \cdot \sin 11° = 0$$
$$F_{AX} = F_S \cdot \sin 11° \tag{1}$$

The moment sum around pivot point $\sum M_A = 0$:

$$-F \cdot b + F_S \cdot \cos 11° \cdot a = 0$$
$$F = \frac{F_S \cdot \cos 11° \cdot a}{b}, \text{ N} \tag{2}$$

For the equilibrium criterion $\sum M_O = 0$ it can be written:

$$F_S \cdot \cos 11° \cdot (b+a) - F_{AY} \cdot b = 0$$
$$F_{AY} = \frac{F_S \cdot \cos 11° \cdot (b+a)}{b}, \text{ N} \tag{3}$$

Tab. 2 shows forces for two planned pivot points.

Table 2 Forces acting on the lever at two pivot points

	Lever length a = 60 mm b = 43,5 mm	Lever length a = 48 mm b = 55,5 mm
F_{AX}/N	81,6	81,9
F_{AY}/N	1002	785,3
F/N	580,9	364,2

3 MATERIALS AND METHODS

The selected materials for the compression tool were the most popular and easily available construction steels S235J2RG (1.0038) which yield strength ranges from σ_Y = 230 - 270 MPa [16, 17], and S355J2 (1.0570) which yield strength ranges from σ_Y = 355 - 400 MPa [16, 18].

It is assumed that both materials have average Young's modulus of $E \approx 210$ GPa at room temperature [16, 19].

Research method is based on the calibration/test of one known configuration in order to verify results, and then conduction series of linear-elastic numerical Finite Element Method (FEM) simulations in order to observe the effect of parameters change in the selected (obtainable) intervals which are related to the tight available workspace in the engine itself, which is shown in the following chapters.

4 DESIGN OF EXPERIMENT/FEM

The 3^3 design of experiment was utilised for the FEM analysis. Fig. 7 shows parameter locations.

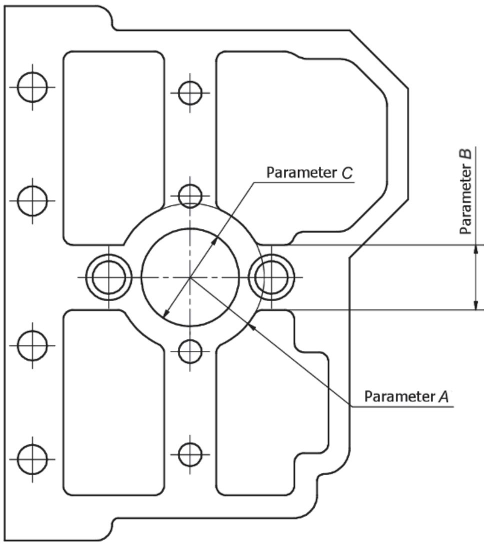

Figure 7 Parameters used for design of experiments

From the Fig. 7 the parameters labelled "A" (outside diameter of the spark plug hole), "B" (bridge width) and "C" (inner diameter of the spark plug hole through which air pressure hose is connected to the spark plug threads). These 3 parameters were varied on three levels each, with respect to plate thickness of 5 mm. In the later parts of this work, the dominant dimension for moment of inertia of the cross section: s is varied on multiple levels. All tool openings are rounded to avoid stress concentrations [20].

Tab. 3shows parameters with respective levels (1, 2, 3). Parameters and their obtainable levels were set as follows: A:{22,75 mm; 25,375 mm; 28 mm}, B:{10 mm; 13,5 mm; 17 mm}, C:{20 mm; 25 mm; 30 mm}.

Table 3 Design of experiment data table

Parameters and their levels			Equivalent stress / MPa		Total displacement / mm
A	B	C	Place 1	Place 2	
1	1	1	115,4	130	0,093315
2	1	1	109,5	113,1	0,0835378
3	1	1	100,3	103,4	0,0761201
1	2	1	110,6	107,6	0,0913467
2	2	1	105,8	105,4	0,0823692
3	2	1	97,2	95	0,0753908
1	3	1	108,2	104,4	0,0897336
2	3	1	103,6	102,3	0,0811979
3	3	1	97,5	103	0,0747208
1	1	2	120,2	124,6	0,0990426
2	1	2	113,4	116,4	0,0877931
3	1	2	104,7	108,5	0,0794324
1	2	2	113,8	106,2	0,0971515
2	2	2	112	103	0,0866143
3	2	2	107,4	97,9	0,0785414
1	3	2	113,1	105,2	0,0951682
2	3	2	110	105,1	0,0853377
3	3	2	100,8	107,1	0,0778638
1	1	3	120,4	131,1	0,105833
2	1	3	119,5	113,2	0,0927699
3	1	3	113,3	104,9	0,0832474
1	2	3	127,5	107	0,103833
2	2	3	121,2	105,8	0,091787
3	2	3	110,1	102,5	0,0822561
1	3	3	119,3	107,1	0,102134
2	3	3	113,8	110,1	0,0903789
3	3	3	109,6	108,2	0,0814401

Fig. 8 shows stressed state of A = 1, B = 1, C = 1 case from Tab. 1. Fig. 9 shows comparison of developed stress field for maximal central ring dimensions obtained by design of experiment data from Tab. 1.

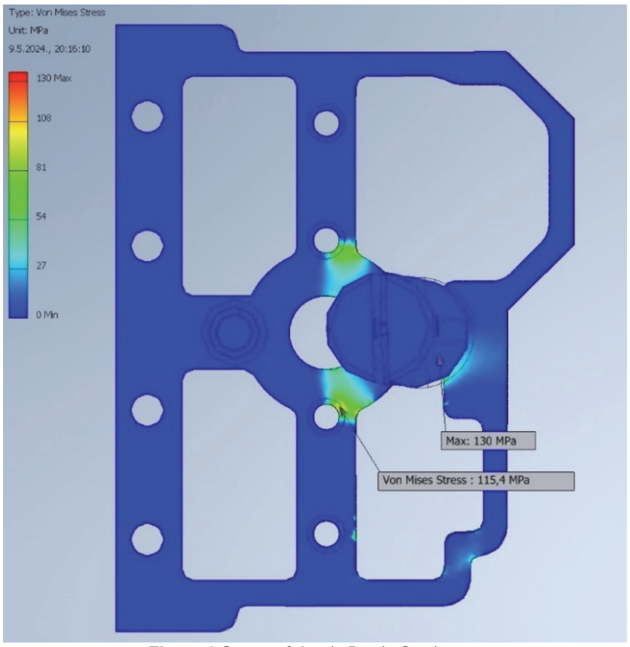

Figure 8 Stress of A = 1, B = 1, C = 1 case

Data for equivalent stress (for place 1 located at the point of mounting screw from Tab. 3 and Fig. 9), is shown in Fig. 10. It is half-normal probability plot of factors with respect to absolute values of their effects.

With normal distribution curve in mind, it can be seen that significant factors for stress are factors A, C

(p = 0,1% or 99,9% confidence). Parameter B is also significant for p = 0,1%, for which F value has to be larger than F = 9,953 [21]; which is surpassed with calculated value F = 10,89 as seen in Tab.4.

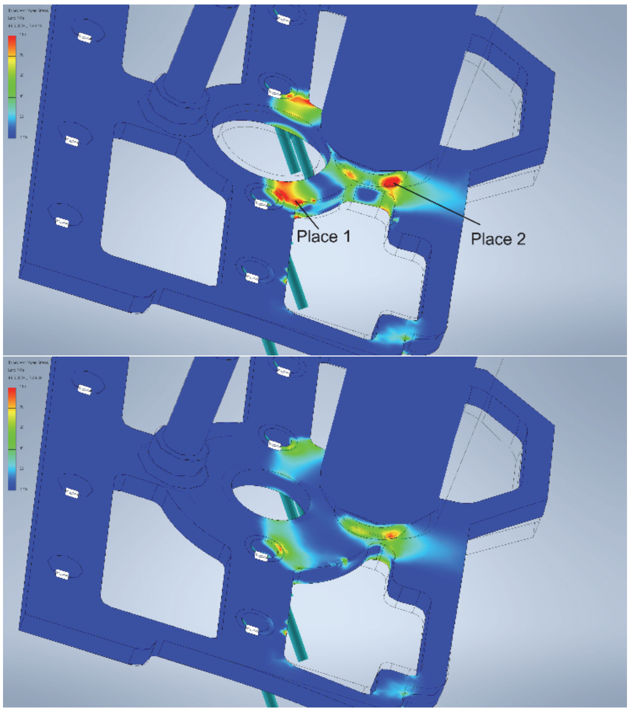

Figure 9 Qualitative stress field size comparison for two extremes (for upper image A = 1, B = 1, C = 3, for lower image A = 3, B = 1, C = 1)

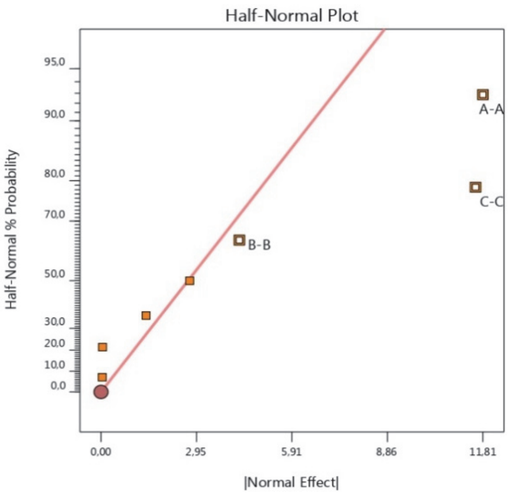

Figure 10 Selected factors with highest effects for equivalent stress on "Place 1" of the compression tool

Tab. 3 shows analysis of variance for the data from Tab. 2

Table 4 ANOVA table for observed "Place 1" from Tab. 2; p = 0,1% (*99,9% confidence)

Source	Sum of squares	df.	Mean Square	F-value	p-value
Model	13980,80	6	231,80	51,07	< 0,0001
Par. A	657,94	2	328,97	72,48	< 0,0001
Par. B	98,89	2	49,44	10,89	0,0006
Par. C	633,98	2	316,99	65,85	< 0,0001
Residual	90,77	20	4,54		
Cor. Total	1481,57	26			

Mathematical model is shown in Tab. 5.

Table 5 Proposed mathematical model for data in Tab. 2

Mathematical model						
	A:		B:		C:	
σ = 111,04+	1:	5,46	1:	1,92	1:	–5,7
	2:	1,04	2:	0,689	2:	–0,444
	3:	–6,493	3:	–2,614	3:	6,147

For example, approximation of stress data in monitored "Place 1" for factors A = 2, B = 1, C = 2 yields expression from Tab. 5:

$$\sigma = 111,04 + 1,04 + 1,92 - 0,444 = 113,6 \text{ MPa} \tag{4}$$

Data from Tab. 3 shows that stress at "place 1" from FEM analysis gives value of 113,4 MPa, which indicates good model approximation. From Tab. 4, it is observable that there is more than 99,9% certainty for proposed mathematical model to be significant since critical F value in literature for 0,1% probability is F = 6,019 (p = 0,1%) and obtained F-value in Tab. 4 is F = 51,07 (much larger than 6,019) [21]. Coefficient of determination for model is R^2 = 0,9387 which also indicates good approximation of the experiment data. Fig. 11 shows graphical results for points of interest (level of factor B = 1).

Overall, these effects of parameters variations on stress intensity were expected, due to moment of inertia of the cross section near the spark plug hole in the tool.

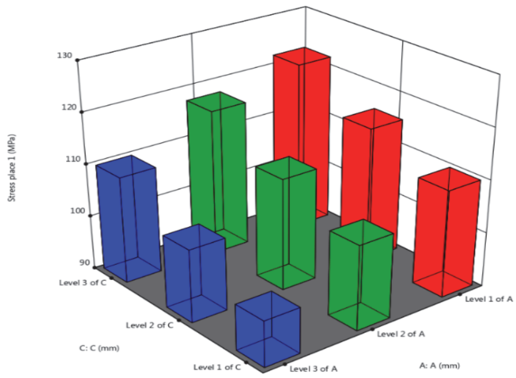

Figure 11 Response stress at "place 1" depending on the A and C parameters from Fig. 7 and Fig. 9

Fig. 12 shows factors with highest effects on equivalent stress in "place 2" of the tool.

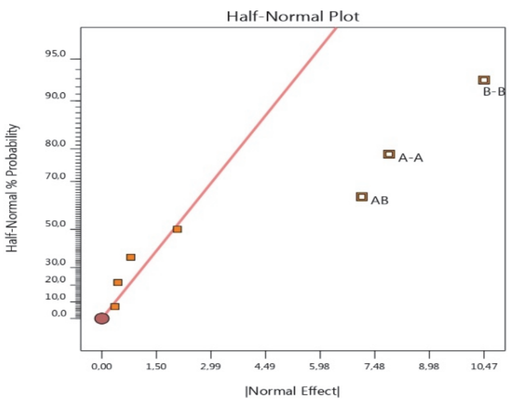

Figure 12 Selected factors which had the highest impact on effects (equivalent stress in "Place 2" from Fig. 9)

Tab. 6 is focused on next point of interest –"place 2", where high stresses were observed. ANOVA for data is given in Tab. 6.

Table 6 ANOVA table for observed "Place 2" stress data from Tab. 2

Source	Sum of squares	df.	Mean Square	F-value	p-value
Model	1748,14	8	218,52	30,43	< 0,0001
Par. A	477,85	2	238,92	33,27	< 0,0001
Par. B	824,47	2	412,24	57,4	< 0,0001
AB - interact.	445,82	4	111,45	15,52	< 0,0001
Residual	129,27	18	7,18		
Cor. Total	1877,41	26			

From statistical tables found in literature [21-23] it can be seen that F-value for the proposed mathematical model with 8 degrees of freedom and 18 degrees of freedom for residuals should be higher than F = 5,763 (p = 0,1%), and it is surpassed by far. Mathematical model as well as parameters have been proven significant (margin set at F = 10,39 for parameters A and B for p = 0,1 %; and for factor interaction AB the margin F-value is set at F = 7,459 for p = 0,1%). These results also make sense physically, as widening of the middle cross section allows for stress field dispersion over a larger surface, and local high stress concentration is diminished. In conclusion, at "Place 2" from Fig. 9, it was advisable to use the widest possible middle section.The resultant mathematical model is too complex to be written here due to parameter interactions, so instead the plot of predicted vs. actual data is shown in Fig. 13. Coefficient of determination for the model is R^2 = 0,9311 indicating good data approximation.

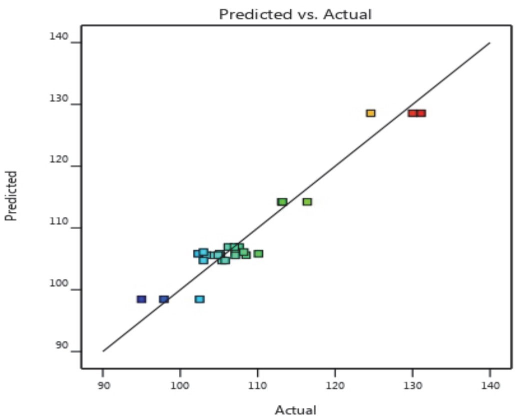

Figure 13 Plot of data predicted by model and actual data

Fig. 14 gives data plot for equivalent stress (factor C data was taken as average).

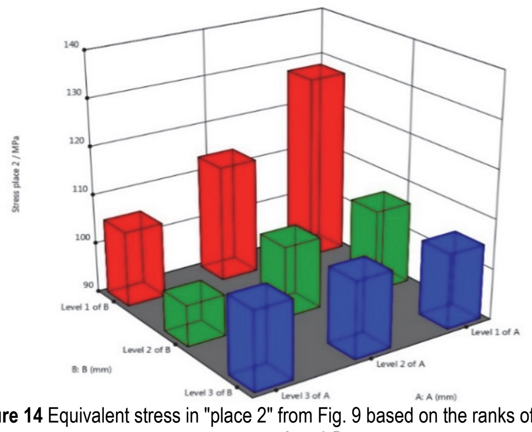

Figure 14 Equivalent stress in "place 2" from Fig. 9 based on the ranks of the parameters A and B

For the tool construction, based on the data the parameters values were selected as: A(3) = 28 mm; B(2) = 13,5 mm; C(1) = 20 mm. This configuration gives one of the lowest equivalent stresses: at "place 1" from Fig. 9, equivalent stress is σ = 97,2 MPa, and at "place 2" equivalent stress is σ = 95 MPa. The tool configuration A(3), B(3), C(1) was not selected, since factor B does not change stress value significantly, but ergonomically if value B = 2 (13,5 mm wide), it gives more manipulation space in the cylinder head for the workers to do repair job.

Subsequent FEM simulations were done for further purpose of multi objective optimisation [24] in order to find out how much benefit on the stress reduction would be obtained if the outside bridge width of the compression tool is increased (shown in Fig. 15).

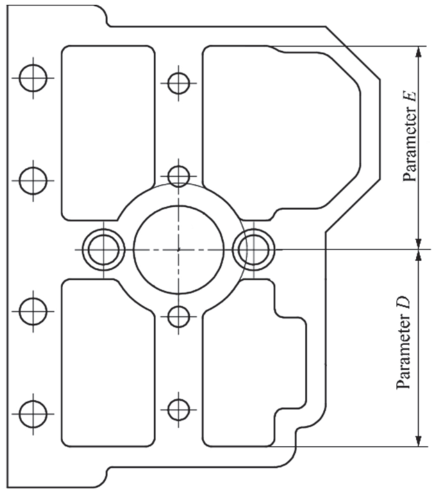

Figure 15 Increased bridge width of compression tool by parameters D, E

The third factor which was changed was sheet metal thickness; in the default version it was selected as 5 mm, and in subsequent numerical simulations the impact of sheet thickness of 3 mm was observed on the stress and the maximal displacement. With thinner sheet metal, the compression tool would be lighter and easier to manufacture. Tab. 7 gives FEM simulations data overview.

Table 7 Equivalent stress and maximal displacements for parameters from Fig. 15

	s = 3 mm	s = 5 mm
Parameter level 1: D = 57 mm E = 59,5 mm	σ = 200,6 MPa	σ = 97 MPa
	u_y = 0,161mm	u_y = 0,065 mm
Parameter level 2: D = 62 mm E = 64,5 mm	σ = 203,6 MPa	σ = 100,1 MPa
	u_y = 0,171mm	u_y = 0,0701 mm
Parameter level 3: D = 67 mm E = 69,5 mm	σ = 208,3 MPa	σ = 98 MPa
	u_y = 0,1823 mm	u_y = 0,0754 mm

The impact of the sheet thickness on equivalent stress is expectable, since area moment of inertia for rectangular profile is increased by the power of 2, i.e. $I_x = (bh^2)/12$. The tool outer bridge did not offer significant reduction of stresses for thickness of 5 mm ($\Delta\sigma_{max}$ = 3,2%). This equivalent stress difference is slightly more observable in the sheet with thickness of 3 mm ($\Delta\sigma_{max}$ = 5,18%). Fig. 16 shows maximal tool displacement under loading for sheet thickness of 3 mm and parameter levels 1 and 3 from Tab. 5 to show contrast in results. Among most popular and easily available construction steels are S235J2RG (1.0038) which yield strength ranges from $R_{p0,2}$ =230 - 270 MPa [16, 17], and S355J2 (1.0570) which yield strength ranges from $R_{p0,2}$ = 355 - 400 MPa [16, 18, 19]. For steel thickness of 3 mm, the equivalent stresses are almost at the yield boundary level for S235J2 (see Tab. 7).

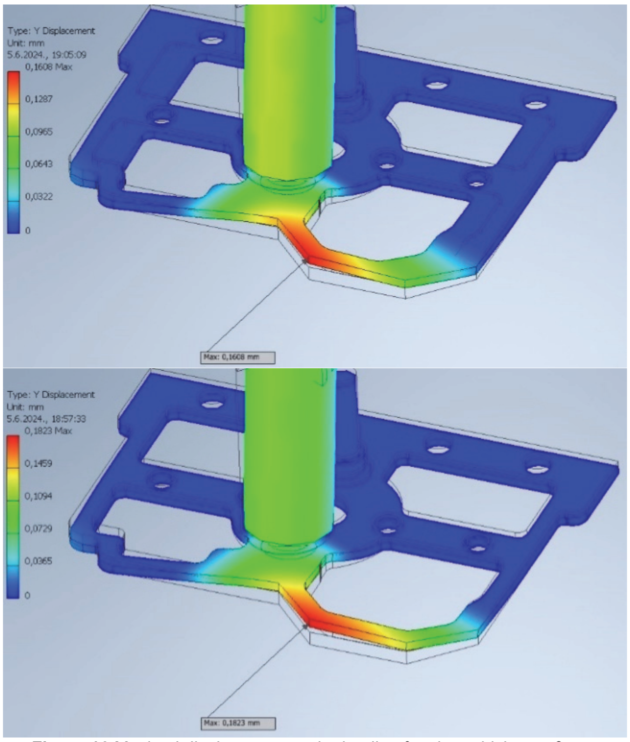

Figure 16 Maximal displacement under loading for sheet thickness 3 mm (u_y = 0,161 mm); and parameters *D, E* on level 1 (upper image). Lower image: parameters *D, E* on level 3, (u_y = 0,182 mm)

In the experimental part, the sheet of 3 mm thick S235J2 material is cut by plasma cutting process and mounted on cylinder head to experimentally measure maximal displacement and compare with FEM analysis results. During work only elastic deformation of the tool body could be seen.

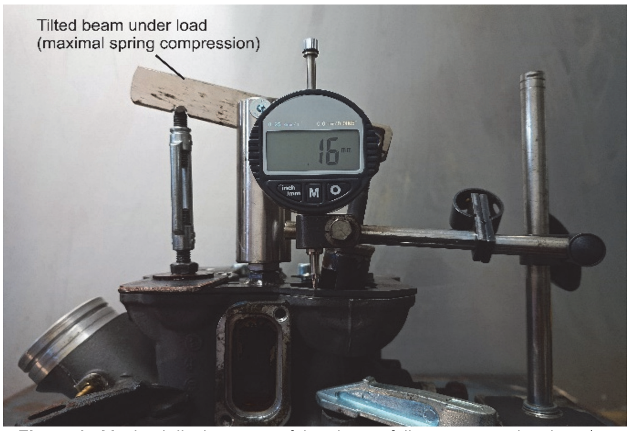

Figure 17 Maximal displacement of the plate at fully compressed springs (as indicated)

5 CONCLUSION

This paper shows refinement in design of holding base plate of spring compressor tool. The spring rates have been measured on Shimadzu machine, cylinder head 2D geometry was obtained and modelled in Autodesk Inventor (3D) based on the valve positions. Based on the available maintenance access area, the base plate configurations were generated as per 3^3 factorial DOE. For each tool configuration, stresses and maximal displacement were obtained, and ANOVA was calculated.

As expected, parameters *A*, *B*, *C* (which create web thickness around spark plug hole) are significant for the stresses. From the standpoint of maximal displacement, in the second DOE it was observed that combination of parameters *A*, *B* and interaction *AB* is significant, which is comparable to the theoretical moment of inertia for rectangular profile. Lastly, in Fig. 16 maximal displacement for the thickest webbing of the base of compression tool gives maximal displacement of u_y = 0,161 mm, which was measured in the experiment but with the two digit precision of the digital dial indicator. This elastic tool deformation is not significant for the technicians, but there is practical side for material recommendation. From Tab. 7 it can be seen that equivalent stress almost reaches yield stress, so it is advisable to use better construction material such as easily available S355J2 (1.0570) or better which will have larger safety factor due to the unaccounted events. It is important to notice that this spring compression tool is designed as light weight tool, with easily accessible port holes for the valve retainers, valve springs and valve seals. In order to keep it light weight and cheap, the thickness of the base plate was kept low.

This research provides design and optimisation of the spring compressor tool, which could be used for the maintenance of worn-out valve stem oil seals without need for cumbersome engine top-end removal. It shortens service time, and maintenance job requires less consumables leading to the better efficiency. For the future research, use of cross-plane members for added rigidity of the tool could be investigated, but with regard to limited workspace and worker ergonomics.

6 REFERENCES

[1] Thomas, R., Sreesankaran, M., Jaidi, J., Paul, D. M., & Manjunath, P. (2016). Experimental evaluation of the effect of compression ratio on performance and emission of SI engine fuelled with gasoline and n-butanol blend at different loads. *Perspectives in Science, 8*, 743-746. https://doi.org/10.1016/j.pisc.2016.06.076
[2] Li, L., Qin, J., Pei, Y., Zhong, K., Zhang, Z., & Sun, J. (2023). The Lean-Burn Limit Extending Experiment on Gasoline Engine with Dual Injection Strategy and High Power Ignition System. *Energies, 16*(15), 5662. https://doi.org/10.3390/en16155662
[3] Marques, J. C., Gasi, F., & Lourenco, S. R. (2024). Biofuel in the Automotive Sector: Viability of Sugarcane Ethanol. *Sustainability, 16*(7), 2674. https://doi.org/10.3390/su16072674
[4] Ye, Y., Hu, J., Zhang, Z., Zhong, W., Zhao, Z., & Zhang, J. (2023). Effect of Different Ratios of Gasoline-Ethanol Blend Fuels on Combustion Enhancement and Emission Reduction in Electronic Fuel Injection Engine. *Polymers, 15*(19), 3932. https://doi.org/10.3390/polym15193932
[5] Kaminaga, T., Yamaguchi, K., Ratnak, S., Kusaka, J., Takashi, Y., Tatsuya, F., & Masahisa, Y. (2019). A Study on Combustion Characteristics of a High Compression Ratio SI Engine with High Pressure Gasoline Injection. *SAE International Technical Paper*, 0106. https://doi.org/10.4271/2019-24-0106
[6] Juwana, W. E., Rachmanto, R. A., Arifin, Z., Yaningsih, I., Tjahjana, D., Suyitno, S., Prasetyo, D., & Nurmansyah, A.

(2024). Influences of Compression Ratio on Performance of Single Cylinder Otto Engine Using E50 Fuel. *International Journal of Mechanical Engineering and Robotics Research, 13*(1), 94-98. https://doi.org/10.18178/ijmerr.13.1.94-98

[7] Gupta, P., Toksa, B., Patel, B., Rushiya, Y., Das, P., & Rahaman, M. (2022). Recent Developments and Research Avenues for Polymers in Electric Vehicles. *The Chemical Record*, 1-40. https://doi.org/10.1002/tcr.202200186

[8] Stojšić, J., Raos, P., Milinović, A., & Damjanović, D. (2022). A Study of the flexural properties of PA12/clay nanocomposites. *Polymers 14*(3), 434. https://doi.org/10.3390/polym14030434

[9] Milojević, S.,Savić, S., Mitrović, S., Marić, D., Krstić, B., Stojanović, B., & Popović, V. (2023). Solving the problem of friction and wear in auxiliary devices of internal combustion engines on the example of reciprocating air compressor for vehicles. *Technical Gazette, 30*(1), 122-130. https://doi.org/10.17559/TV-20220414105757

[10] Milojević, S., Savić, S., Marić, D., Stopka, Ondrej., Krstić, B., & Stojanović, B. (2022). Correlation between Emission and Combustion Characteristics with the Compression Ratio and Fuel Injection Timing in Tribologically Optimized Diesel Engine. *Technical Gazette,* 29(4), 1210-1219. https://doi.org/10.17559/TV-20211220232130

[11] Milojević, S., Glisović, J., Savić, S., Bošković, G., Bukvić, M., & Stojanović, B. (2024). Particulate Matter Emission and Air Pollution Reduction by Applying Variable Systems in Tribologically Optimized Diesel Engines for Vehicles in Road Traffic. *Atmosphere, 15*(2), 184. https://doi.org/10.3390/atmos15020184

[12] Mofidi, M., Kassfeldt, E., & Prakash, B. (2008).Tribological behaviour of an elastomer aged in different oils. *Tribology International, 41*(9-10), 860-866. https://doi.org/10.1016/j.triboint.2007.11.013

[13] Patel, H., Salehi, S., Ahmed, R., & Teodoriu (2019). Review of elastomer seal assemblies in oil & gas wells: Performance evaluation, failure mechanisms, and gaps in industry standards. *Journal of Petroleum Science and Engineering, 179*, 1046-1062. https://doi.org/10.1016/j.petrol.2019.05.019

[14] Glavaš, H., Karakašić, M., Kljajin, M., & Desnica, E. (2021). Essential Preventive Automobile Maintenance during a Pandemic. *Technical gazette, 28*(6), 2190-2199. https://doi.org/10.17559/TV-20201229130413

[15] Mikić, D., Desnica, E., Ašonja, A., Epifanic Bajic, V., & Stojanovic, B. (2016). Reliability analysis of ball bearing on the crankshaft of piston compressors. *Journal of the Balkan Tribological Association,* 22(4), 5060-5070. https://doi.org/10.1016/j.petrol.2019.05.019

[16]Spittel, T. & Spittel, M. (2007). *Group VIII: Advanced Materials and Technologies - Metal Forming Data part 1 - ferrous alloys*. Landolt-Börnstein, Numerical Data and Functional Relationships in Science and Technology. Springer.

[17] Correia, J. A. F. O., da Silva, A. L. L., Xin, H., Lesiuk, G., Zhu, S. P., de Jesus, A. M. P., & Fernandes, A. A. (2021). Fatigue Performance Prediction of S235 Base Steel Plates in the Riveted Connections. *Structures,* (30), 745-755. https://doi.org/10.1016/j.istruc.2020.11.082

[18] Steel navigator. Material steel grade S355J2 data. URL: https://steelnavigator.ovako.com/steel-grades/s355j2/pdf (accessed 13.1.2025).

[19] Milovanović, V., Arsić, D., Milutinović, M., Živković, M., & Topalović, M. (2022). A Comparison Study of Fatigue Behavior of S355J2+N, S690QL and X37CrMoV5-1 Steel. *Metals, 12*(7), 1199. https://doi.org/10.3390/met12071199

[20] Radojković, M., Stojanović, B., Milojević, S., Marić, D., Skulić, A., & Krstić, B. (2023). Square Openings as Sources of Stress Concentration in Parts of Machines and Devices. *Technical Gazette, 30*(2), 474-480. https://doi.org/10.17559/TV-20220603080026

[21] Anderson, M. & Whitcomb, M. (2007). *DOE simplified - practical tools for effective experimentation*. CRC press, New York.

[22] Oehlert, G. (2010). *A first course in design and analysis of experiments.* University of Minnesota, Minnesota. ISBN 0-7167-3510-5.

[23] Jiju, A. (2023). *Design of experiments for engineers and scientists*. Oxford, United Kingdom: Elsevier.

[24] Gajević, S., Marković, A., Milojević, S., Ašonja, A., Ivanović, L., & Stojanović, B. (2024). Multi-Objective Optimization of Tribological Characteristics for Aluminum Composite Using Taguchi Grey and TOPSIS Approaches. *Lubricants, 12*(5), 171. https://doi.org/10.3390/lubricants12050171

Contact information:

Josip CUMIN, assistant professor
(Corresponding author)
University of Slavonski Brod, Mechanical Engineering Faculty,
Trg Ivane Brlic Mazuranic 2, Slavonski Brod
E-mail: jcumin@unisb.hr

Dejan MARIĆ, assistant professor
University of Slavonski Brod, Mechanical Engineering Faculty,
Trg Ivane Brlic Mazuranic 2, Slavonski Brod
E-mail: dmaric@unisb.hr

Daniel NOVOSELOVIĆ, associate professor
University of Slavonski Brod, Mechanical Engineering Faculty,
Trg Ivane Brlic Mazuranic 2, Slavonski Brod
E-mail: dnovoselovic@unisb.hr

Tomislav ŠOLIĆ, assistant professor
University of Slavonski Brod, Mechanical Engineering Faculty,
Trg Ivane Brlic Mazuranic 2, Slavonski Brod
E-mail: tsolic@unisb.hr